Bull Earthquake Eng (2017) 15:5167–5189
DOI 10.1007/s10518-017-0182-y

ORIGINAL RESEARCH PAPER

Seismic performance of RC buildings during the M_W7.8 Muisne (Ecuador) earthquake on April 2016: field observations and case study

Alexander Kagermanov[1] · Paola Ceresa[1] · Enrique Morales[2] · Jose Poveda[1] · Jerome O'Connor[2]

Received: 12 January 2017 / Accepted: 21 June 2017 / Published online: 28 June 2017
© Springer Science+Business Media B.V. 2017

Abstract The $M_w = 7.8$ Muisne event of April 16, 2016 occurred on Saturday at 18:58:37 local time off-shore of the west coast of northern Ecuador. Several cities in the province of Manabí were directly affected and a state of emergency was declared in six provinces encompassing a total area of 70,000 km^2. The building stock was severely damaged. 80% of the buildings were destroyed in the city of Pedernales, while several multi-storey reinforced concrete structures totally collapsed in the cities of Manta and Portoviejo. Field observations on the seismic performance of reinforced concrete buildings inspected by the authors are presented in this paper. Also, numerical results from three-dimensional pushover analysis of a representative case study building are discussed. The effect of corrosion and masonry infills, which played a key role in the observed damage, was directly taken into account in the analytical model.

Keywords Ecuador earthquake · Reinforced concrete frames · Seismic performance · Corrosion · Masonry infills

1 Introduction

The western coast of Ecuador belongs to the South-American seismic arc which extends from southern Chile towards Panama in Central America. In this region the oceanic Nazca plate subducts eastward beneath the continental South-American plate, with convergence rates varying from 80 mm/year in the south to approximately 70 mm/year in the north (US Geological Survey 2016). Figure 1 shows the epicenter of $M_w \geq 7$ events located along this boundary. This convergent process is one of the most active worldwide, being

✉ Alexander Kagermanov
alexander.kagermanov@umeschool.it

[1] Scuola Universitaria Superiore (IUSS), Pavia, Italy

[2] University of Buffalo, New York, NY, USA

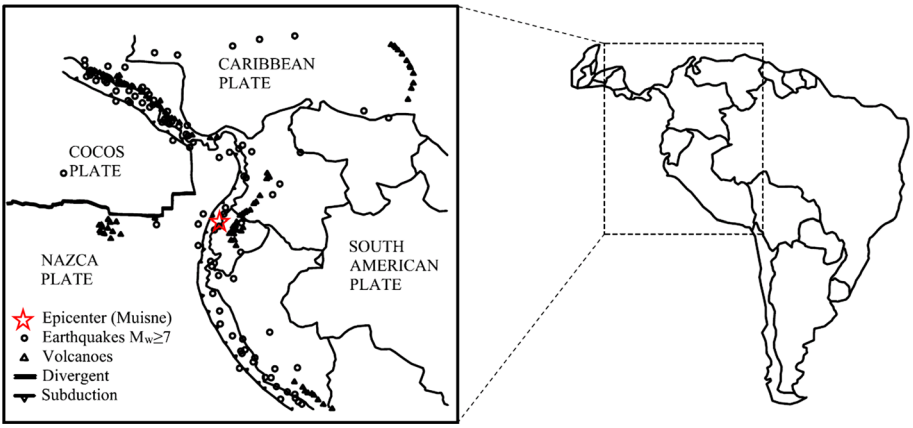

Fig. 1 Seismic and tectonic setting in South American showing $M_w \geq 7$ events and active volcanoes located along the South American arc. Adapted from (US Geological Survey 2016)

responsible for creating the Andes Mountains, the active volcanic chain along its deformation front and some of the strongest earthquakes, such as the largest ever recorded $M_w = 9.5$ event of 1960 in southern Chile (US Geological Survey 2016).

Ecuador has a long history of large subduction interplate thrust earthquakes, such as the 1906 M8.5 earthquake near Esmeraldas and the 1979 M8.2 Tumaco earthquake between the Ecuador and Colombia coasts, both followed by devastating tsunamis. The 1998 M7.2 earthquake near Bahía de Caráquez caused similar damage patterns to the 2016 Muisne earthquake (Earthquake Engineering Research Institute 2016a), although of lesser extent. Some important earthquakes also occurred along the Andes Mountains, such as the 1987 $M_s = 6.1$ and $M_s = 6.9$ sequence of earthquakes in the Province of Napo in northeastern Ecuador. This event caused major damage to the Trans-Ecuadorian Pipeline carrying oil 260 miles from the eastern oil fields to the port of Esmeraldas in the Pacific Ocean (Earthquake Engineering Research Institute 2016b).

2 The Muisne earthquake of April 16th, 2016: overview

The Muisne Earthquake of $M_w = 7.8$ occurred on Saturday 16th of April, 2016 at 18:58:37 local time off-shore of the west coast of northern Ecuador near the boundary zone between the Nazca and the South-American plates (0.371°N, 79.94°W), at a depth of 19 km (US Geological Survey 2016). A $M_w = 5$ foreshock was reported, as well as over 1000 aftershocks within 15 days after the main shock (Instituto Geofísico Escuela Politécnica Nacional de Ecuador (IGEPN) 2016). The earthquake was the result of shallow thrust faulting on the plate boundaries of the Nazca and South-American plates, where the former subducts eastward at a rate of 61 mm/year (US Geological Survey 2016). According to recent empirical studies on source dimension scaling in subduction zones (Strasser et al. 2010), events of this magnitude typically correspond to a fault rupture area of 120×70 km^2.

The earthquake directly affected the coastal provinces of Manabí and Esmeraldas covering an area of 35,000 km^2, with a population of almost 2 million people. Major damage occurred in the cities located along the cost-line, such as Pedernales, Bahía de

Caráquez and Manta, which are considered popular touristic destinations with several multi-storey RC apartment and hotel buildings. The maximum seismic intensity reached 9 EMS in Pedernales and Chamanga, and 8 EMS in Manta (Instituto Geofísico Escuela Politécnica Nacional de Ecuador (IGEPN) 2016). Some inland cities were severely affected as well, such as the province capital Portoviejo which reached 8 EMS, and where local site amplification took place due to the presence of soft soils deposits along the river Portoviejo. Also in the city of Guayaquil, the most populated of Ecuador and located 270 km from the epicenter, the presence of deep plastic clays caused local site amplification comparable to that of Mexico City, resulting in an intensity of 6 EMS. Table 1 reports some statistics regarding exposure and loss consequences for several affected areas (see also Fig. 3) (Wikipedia the Free Encyclopedia 2016). For each canton, the number of buildings with moderate (MD), severe (SD) and collapse (CD) damage is indicated according to the satellite-based assessment reported in United Nations Institute for Training and Research UNITAR (2016). The city of Pedernales, located right on the fault rupture projection and 30 km from the epicenter, was subjected to a direct hit damaging 80% of the building stock. For large-magnitude events like the present one, with source dimensions of more than just a few kilometers, the epicentral distance requires careful interpretation. For example, the city of Esmeraldas, located only 70 km from the epicenter, was damaged to a lesser extent than Chone, located at 120 km, while being Esmeraldas more populated than Chone. The closest distance to the surface projection of the fault rupture plane, R_{jb} (Joyner–Boore distance), correlates better with the observed damage in this case, which was 25 and 0 km for Esmeraldas and Chone, respectively. The cities of Portoviejo and Manta were both located at similar R_{jb} distances. However, Portoviejo was severely affected due to local site conditions, whereas in Manta the fewer collapses occurred in Tarqui due to poor quality construction.

The distribution of buildings in the country according to the type of construction material and census date is shown in Fig. 2 (Instituto Nacional de Estadística y Censos INEC 2016a, b, c, d). It is noted that the majority of structures are reinforced concrete, usually located in large urban areas, whereas adobe, timber and cane houses are more characteristic of rural areas. In the 2010 census, the contribution of rural population to the national census had significantly increased, causing a decrease in the percentage of concrete construction versus vernacular one. The majority of people still live in urban areas, 9 million versus 5 million in rural areas, and in reinforced concrete structures.

The poor structural performance of buildings during the Muisne earthquake was mainly due to the existence of many non-engineered structures and common problems of

Table 1 Exposure and loss consequence statistics after the earthquake

Canton	ED (km)	R_{jb} (km)	Area (km^2)	Population	Fatalities	HU	MD	SD	C
Esmeraldas	70	25	1351	190,000	1	55,000	2	0	6
Pedernales	30	0	1932	55,000	173	14,000	30	38	57
Chone	120	0	3570	125,000	6	36,000	64	36	62
Sucre	120	0	764	60,000	28	14,000	114	107	70
Manta	170	40	309	225,000	210	67,000	30	10	7
Portoviejo	170	40	967	280,000	133	82,000	267	83	87

ED/R_{jb}, epicentral distance/closest distance from fault rupture projection to canton capital; HU, house units; MD, moderate damage; SD, severe damage; C, collapse

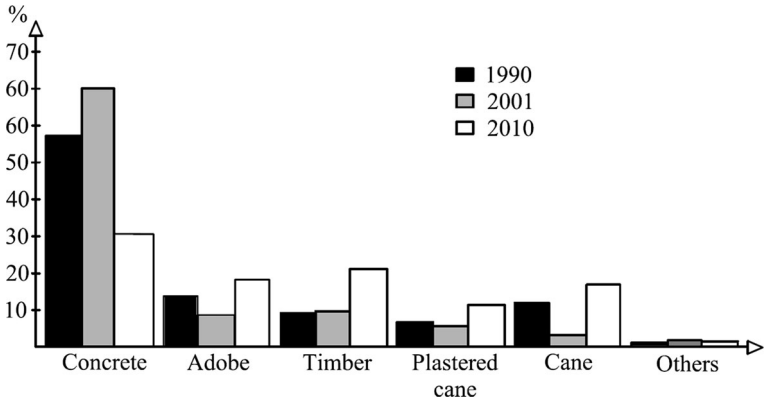

Fig. 2 Distribution of buildings in the country according to the type of construction material (Instituto Nacional de Estadística y Censos INEC 2016a, b, c, d)

irregularity and limited ductility in the engineered ones. This concerned not only residential buildings but also essential facilities such as hospitals and schools. Although none of the hospitals collapsed, 22 were left inoperative in the province of Manabí and Esmeraldas due to severe damage to non-structural components (Secretaría de Gestión de riesgos 2016). Medical assistance was provided from temporary shelters, resulting in overcrowding, lack of sanitation and increasing risk of epidemic disease transmission in the days following the earthquake.

Additional damage concerned landslides and liquefaction influenced by the long duration of ground shaking and low effective stress-state of the soil following the rainy season of El Niño. Over 500 cases of landslides and liquefaction have been reported, most of them in Bahía de Caráquez and the port of Manta (United Nations Institute for Training and Research UNITAR 2016). Lateral spreading of several bridge approaches, with settlements between 30 and 60 cm in some cases, caused partial disruption of the transportation system hindering access to the affected areas during the emergency response. The overall performance of bridges was satisfactory, except the collapse of an overpass reinforced concrete structure in the city of Guayaquil. Water and electricity supply were also affected, leaving many people without potable water for several days. The earthquake left 660 fatalities, over 16,000 injured and 20,000 displaced. The economic loss was estimated as 3 billion US dollars (Secretaría de Gestión de riesgos 2016).

3 Ground motions and response spectra

The present earthquake was the largest ever registered by the National Network of Accelerographs of Ecuador (RENAC), maintained by the Institute of Geophysics of the National University of Ecuador (IGEPN). The majority of stations are located along the Andes Mountains in Central Ecuador and the western coast. A total of 30 stations recorded the event, 21 from RENAC and 9 from external collaborators, such as the oil company "Oleoductos de Crudos Pesados", the closest station being 30 km from the epicenter in the city of Pedernales. Some of the stations do not stream continuously, hence manual collection of data from the site was required. Data processing consisted of baseline correction, envelope multiplication with a 5% cosine taper function and no filtering (Instituto

Geofísico Escuela Politécnica Nacional de Ecuador (IGEPN) 2016). Records were finally made available about 3 weeks after the main shock. Unfortunately, no information regarding soil profiles at the recording sites is available, which imposes a major difficulty in performing detailed analysis and interpretation of the recorded accelerograms.

The PGAs recorded at the stations that registered important levels of shaking during the main shock are shown in Fig. 3. It is observed that most of the seismic energy propagated in the north–south direction following the fault rupture projection (US Geological Survey 2016), whereas significant attenuation took place in the west–east direction. Similar attenuation effects in volcanic regions have been reported in other tectonic environments (McVerry et al. 2006). In the city of Pedernales, maximum horizontal PGA values reached 1.4 g for the EW component and 0.7 g for the vertical component. In Manta and Portoviejo, maximum horizontal PGA components reached 0.51 and 0.37 g, respectively, both in the NS direction. The ratio of the vertical-to-horizontal PGA for the near-field record in Pedernales was 0.5, and 0.3 and 0.27 for the far-field records in Manta and Portoviejo, respectively. Note these values are lower than the 2/3 design rule used in the Ecuadorian building code for the vertical design spectrum, suggesting that the effect of the vertical component should not be critical for new, code compliant structures. The recorded PGA values were shown to correlate well with recent studies on ground motion prediction equations for interface events in subduction zones [Instituto Geofísico Escuela Politécnica Nacional de Ecuador (IGEPN) 2016; Abrahamson et al. 2016].

The recorded acceleration time histories in Pedernales (APED) and Manta (AMNT), and the corresponding cumulative Arias Intensities (AI) are shown in Fig. 4. It can be noticed that the 1.4 g PGA recorded in Pedernales seems to be related to very high-frequencies, implying that it might have been lower, had the records been filtered. The duration of ground shaking, measured as the interval from 5 to 95% of the total AI (significant duration D_s) of the strongest component, was 29 s in Pedernales, and 17 s and 14 s in Manta and Portoviejo, respectively. The enormous amount of energy release and greater duration in Pedernales is evident from Fig. 4. The duration of ground shaking likely affected the extent of landslides and liquefaction. Thresholds of about 0.25-0.3 m/s of AI have been suggested for landslide triggering (Harp and Wilson 1995), which are clearly exceeded for Pedernales and Manta.

The elastic acceleration response spectrums for 5% damping recorded at the stations APED, AMNT and APO in the east–west (E), north–south (N) and vertical (V) directions are compared in Fig. 5. Also shown is the design spectrum for a 475-year return period

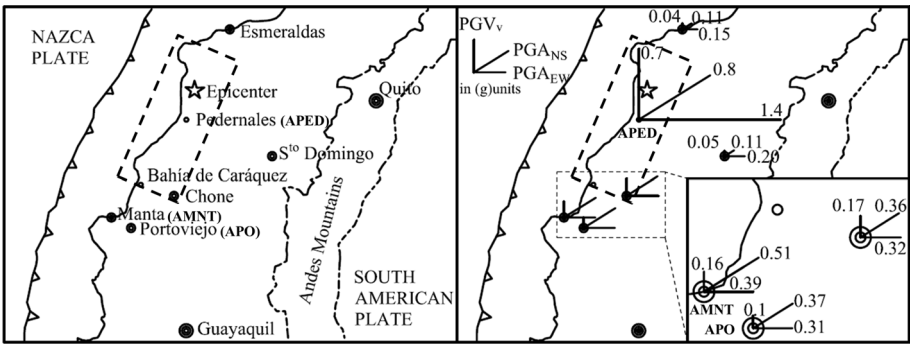

Fig. 3 Fault rupture projection and PGAs recorded during the Muisne Earthquake [US Geological Survey 2016; Instituto Geofísico Escuela Politécnica Nacional de Ecuador (IGEPN) 2016]

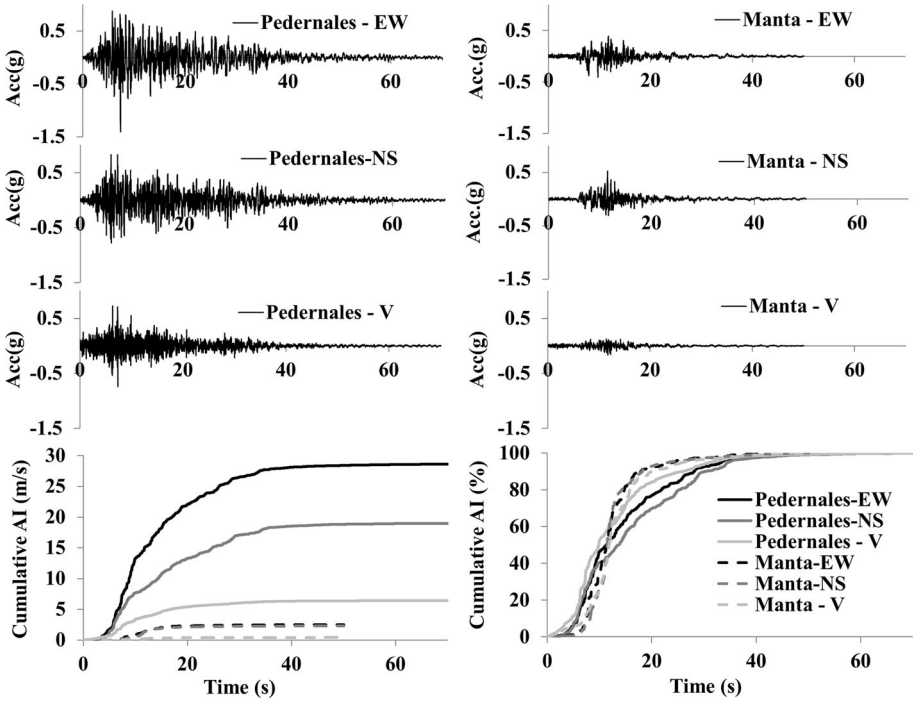

Fig. 4 Arias Intensity plots and ground motions recorded in the cities of Pedernales (*left*) and Manta (*right*)

according to the National Building Code of Ecuador (NEC-2014) for three different site classes: soil C (760 m/s $\geq V_s >$ 360 m/s), soil D (360 m/s $\geq V_s >$ 180 m/s) and soil E (180 m/s $\geq V_s$) (Norma Ecuatoriana de la Construcción 2014). The design spectrum is anchored at the PGA on solid rock, given as 0.5 g for the coastal region, multiplied by the site coefficient F_a (Norma Ecuatoriana de la Construcción 2014). The latter depends on the site class and ground shaking intensity on bed rock, similarly to the ASCE code [ASCE (American Society of Civil Engineers) 2010]. The spectral amplification factor defining the maximum acceleration plateau is $\eta = 1.80$ for the coastal region. For Pedernales (Fig. 5), the recorded maximum spectral ordinates exceed by a factor of 3 those of the design spectrum, particularly in the period range from 0 to 1 s, whereas in Manta the spectral intensity level was relatively close to the design level. In Portoviejo, local site conditions resulted in spectral amplification at T = 0.45 s by about 5.7 times the PGA, which clearly cannot be captured by the NEC-2014 site coefficients. The 5% elastic response spectrum for the vertical components is also reported in Fig. 5. The high-frequency content can be clearly appreciated, being the maximum spectral ordinate about 2.6 g at T = 0.1 s in Pedernales.

It is important to mention that the design spectrum aims at representing multiple earthquake scenarios based on a probabilistic seismic hazard assessment (PSHA). Hence, comparison with individual records must be made with care and does not necessarily invalidate the design spectrum. The 2001 Ecuadorian Building Code (CEC) was the first to include a detailed PSHA at a national scale, undertaken by the IGEPN. A total of 53 known seismic sources were modeled, and a homogenized catalogue with events between magnitude 3.9 and 8.6 was used. State-of-the-art ground motion prediction equations were used

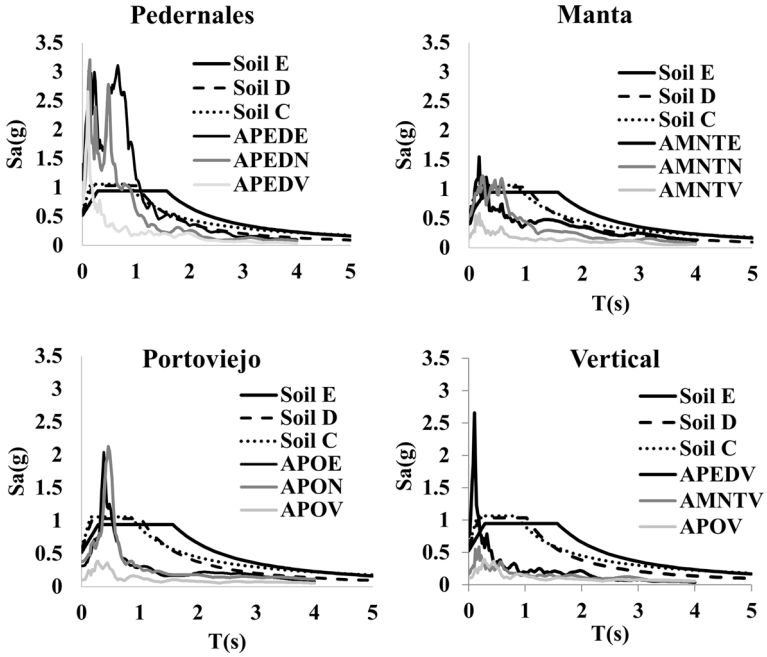

Fig. 5 Elastic response spectrums at 5% damping and the design spectrum at 10% probability of exceedance in 50 years as per NEC-2014

for subduction and crustal earthquakes, adjusted to the available acceleration records in Ecuador. The PGA at 475-year return period on solid rock assigned to the coastal region was 0.4 g, which was raised to 0.5 g in the NEC-2014 following an update after the 2010 Earthquake of Haiti.

First seismic design considerations appeared in the National Construction Code released in 1951 after the devastating $M_w = 6.8$ Ambato Earthquake in 1949. The document was made mandatory, however its practical application was very limited and in 1976 widespread damage occurred during the $M_w = 6.7$ Earthquake, 15 km from the city of Esmeraldas, including total collapse of several non-ductile reinforced concrete frames. In 1977 the Ministry released the Official Code of Construction based on the ACI 318-71, which included several advanced concepts related to design and detailing for ductile behavior, consideration of the dynamic properties of the structure, its energy dissipation capacity and local site conditions in the calculation of the base shear coefficient (Neinhuys et al. 1976). Capacity design principles were first introduced in the recent NEC-2014 code. Its predecessor, the 2001 Ecuadorian Building Code (CEC), did not explicitly consider capacity design, although reference was made to ACI standards which did consider it. However, its application is rather questionable and might be limited to a few qualified design offices. Overall the NEC-2014 and its predecessors can be considered as updated design standards, closely following the Colombian (NSR-10) and American (ASCE7-10) documents, as well as other American standards such as FEMA, NEHRP and ATC. As will be shown later, the significant extent of damage observed in the present event is more related to code enforcement and construction control issues, rather than state of the knowledge in Ecuador.

4 Performance of RC building structures

4.1 General observations

Most of the building stock in the affected urban areas is composed of RC frames with unreinforced masonry (URM) infills and waffle or flat slabs. Shear walls, precast or steel structures are very rare. No distinction is made between gravity and lateral load resisting frames in Ecuador, as it is common practice in the US. Instead, all frames contribute to the gravity and lateral load resisting system, resulting in greater axial-load ratios in the columns than when the two systems are decoupled. Unfortunately, due to the inherent stiffness of the slab, slenderness of columns and poor detailing of the column-to-slab connections, most of the plastic hinges developed in the columns precluding the formation of the weak beam-strong column mechanism. This, accentuated by heavy partitions, soft-storeys and poor material quality, resulted in the total collapse of several structures which were either old and designed according to past standards, or non-code-compliant. The performance of new code-compliant structures was in general satisfactory.

The period of construction is rather heterogeneous, ranging from old (about 50 years old), non-engineered low-rise buildings to more modern apartments with up to 16 storeys. Smooth rebars were observed in some of the old buildings, which had been used in Ecuador until the 70 s, although the change to deformed rebars was gradual and more delayed in the rural areas. Modern buildings tend to have deep beams, as opposed to old ones with concealed beams within flat slabs, which helps developing hinges at beam ends if capacity design rules and appropriate detailing is followed.

Most of the buildings are designed as bare frames, without considering frame-infill interaction. Seismic regulations addressing this issue do not exist, neither for analysis nor construction. Hence, construction and detailing is left to the local workmanship. Infills usually consist of hand-compacted baked clay bricks or concrete/cement mortar blocks, and sometimes hollow clay units. Other systems such as gypsum partitions, widely used in the US, are not common practice. Infills are constructed after casting beams and columns without any vertical confinement, as opposed to Colombian and Chilean practice, and they are neither reinforced nor anchored to the frame, except in a few modern buildings. As a result, infills are very weak, leading to increased frame flexibility and widespread in-plane and out-of-plane damage. Note that infill damage initiates much earlier than frame damage, at about 0.1% inter-storey drift, whereas yielding of the frame typically occurs at about 1–2%, as also shown for the case study building in this paper.

4.2 Observed case studies

Some typical residential buildings that were found particularly vulnerable to the ground shaking are shown in Fig. 6. The five-storey RC building in Fig. 6a is located in Tarqui, which was the most affected area in Manta declared as ground zero zone. The building presented a soft-storey at the ground level due to removal of masonry infills from the facade plane. Spalling of concrete cover and 20 mm thick plaster was observed at the bottom of the columns, as well as corrosion of longitudinal and transverse reinforcement (Fig. 6b). Some of the ground-floor-columns had been strengthened, hence failure localized immediately after the section reduction in the form of concrete crushing (Fig. 6c). Also note the out-of-plane damage to the infills at the roof level, where the typical layout of the columns was changed during the construction of an additional storey. This type of

Fig. 6 5-Storey RC building with masonry infills located in Tarqui (Manta) (**a**), and its damage to the ground-floor-columns (**b**, **c**)

structural alterations, whereby additional stories are added at different construction periods without reassessment of the structural performance, was commonly observed. This intervention increases the mass and axial load in the existing columns, and introduces stiffness and strength irregularities which can result in undesirable performance.

Fig. 7 Soft-storey buildings in Manta (**a**), damage to the columns (**c**) and partitions (**d**)

Further examples of soft-storey frame buildings are shown in Fig. 7a, b. All of these structures were located in Manta, where ground accelerations close to the 475-year design level were recorded. Typical column reinforcement consisted of 14 mm longitudinal bars with 8 mm stirrups spaced at 200–250 mm (250 mm in Fig. 7c), although the current code prescribes a minimum spacing of 100 mm within the plastic hinge region L_o, with L_o - $\geq$ 450 mm. Figure 7d shows some damage to masonry partitions at the ground level of the building in Fig. 7b, where most of the lateral drift was concentrated.

The four-storey building in Fig. 8 was located also in Manta. It is an interesting case of structure that performed relatively well despite presenting several structural and architectural deficiencies, such as removal of an intermediate column at the ground level (Fig. 8b) and the use of heavy column cladding (Fig. 8c). Important detailing deficiencies were found in the column end regions, with stirrups bent at 90° with 300 mm spacing (Fig. 8e, g), and longitudinal bars cut off (Fig. 8e), thus impairing the bending moment capacity in the region of highest moment demand, which ideally should remain elastic according to capacity design principles. According to the current Ecuadorian code, lap splices of column longitudinal bars must occur at column mid-height, outside the plastic hinge regions. Moreover, significant corrosion and loss of bond was observed in Fig. 8e. Despite these deficiencies, the structure did not lose its vertical load carrying capacity, which was partially transferred to the masonry infills.

Extensive corrosion was observed in many structures due to the hot, humid and salty conditions of the region. Chloride was present not only in the environment but also in the concrete itself, since many buildings had been built with beach sand, as locally reported.

Fig. 8 4-storey RC building with several deficiencies located in Manta (**a**), structural irregularities and heavy cladding (**b**, **c**), and detailing deficiencies (**d**, **e**, **f**)

Moreover, insufficient concrete cover, usually <20 mm, accelerated the degradation process. Cover concrete/plaster spalling and fracture of stirrups at the ground-floor-column of an old two-storey building is shown in Fig. 9a. This failure occurred at column mid-height as a result of extensive corrosion and expansion of reinforcement. Also, several columns were found excessively slender (20 × 20 cm^2 in Fig. 9a). The current NEC-2014 code specifies minimum column dimensions of 30 × 30 cm^2. An electrical RC post with a hollow circular cross-section is shown in Fig. 9b, which failed due to insufficient anchorage length and corrosion of the rebars. Note also that smooth rebars were used in Fig. 9a.

The Ceibo Dorado Hotel, constructed in 2010 and located in the ground zero zone in Portoviejo, is shown in Fig. 10a. It consists of an L-shaped 7-storey RC structure with no seismic joints between adjacent blocks. Damage to interior masonry partitions and exterior infills was observed mostly at lower storeys. Structural irregularities introduced by the interior staircase resulted in concrete crushing and flexure-shear cracking of the landing slab (Fig. 10b). Also, signs of flexural yielding and beam elongation were noticed in some beams framing into perimeter joints (Fig. 10c), likely accentuated by torsional effects. Overall the structure performed relatively well and without any apparent permanent drift, despite being its natural period close the local amplification peak at 0.5 s in Portoviejo.

The 15-storey hotel Oro Verde, built in the late 1970s and located at the beach front in Manta, is shown in Fig. 11a. It is a good example of a long period structure with damage at intermediate storeys, presumably due to higher mode effects. The damage consisted of diagonal shear cracks localized in masonry infills (Fig. 11a). Note that the structure is isolated from neighboring buildings, hence no group interaction occurred.

An impressive local collapse was triggered in the Mutualista Pichincha building, a 10-storey RC structure built in the late 1980s and located in downtown Portoviejo (Fig. 11b). The upper three storeys collapsed on top of the lower part of the building across a soft-storey plane, likely influenced by the short-column effect from interaction with external cladding panels (see close-up). Local witnesses reported that the upper part was slowly "creaking" with every aftershock. The building was recently demolished under controlled implosion.

The Supreme Court building in Portoviejo, constructed in 2002 (Fig. 12a), is a 9-storey RC structure with 3 independent adjacent blocks, stiff rectangular columns (0.5 × 1 m^2)

Fig. 9 Damaged column (**a**) and collapsed electrical post (**b**)

Fig. 10 7-storey Hotel Ceibo Dorado in Portoviejo overall damage (**a**), damage to the staircase (**b**) and perimetral beams (**c**)

and 4.5 m long shear walls. The structure did not suffer any important damage, with only minor damage at the construction joint due to pounding between slabs (Fig. 12b). However, non-structural damage was important. Diagonal shear cracks were noticed in the facade masonry, consisting of hollow concrete bricks. Damage to the contents, e.g. overturning of bookshelves, was significant in the upper storeys (Fig. 12c) where greater floor accelerations occurred, whereas in the lower storeys drift sensitive components were more affected (Fig. 12d).

As previously mentioned, many hospital facilities were left inoperative due to extensive non-structural damage, although none of them completely collapsed. The structural system was similar to that of residential buildings, i.e. RC frames with URM infills, but with stiffer and stronger members resulting in higher floor accelerations and wide-spread damage to acceleration sensitive components, such as medical equipment. The Miguel Hilario Alcivar hospital in Bahía de Caráquez (Fig. 13) represents an interesting example of retrofitted structure after the 1998 Bahía de Caráquez earthquake. Retrofitting consisted in the addition of six shear walls and jacketing of some perimeter columns. Minor structural damage occurred during the present earthquake, with some spalling of plaster and concrete cover in the boundary wall elements (Fig. 13c). However, damage to the contents and the psychological impact on people located in the building during the earthquake left it inoperative (Fig. 13b).

The Solca Hospital in Portoviejo was left only 40% operative after the earthquake. The building was built in early 2000s and it consisted of multiple, up to three-storey units separated by expansion joints. One of the units presented an additional two-storey tower which did suffer extensive damage to the non-structural and structural components (Fig. 14a). In Fig. 14b, damage to a non-structural column of an interior infilled frame is shown. The interior column of the tower (Fig. 14c) presented insufficient number of

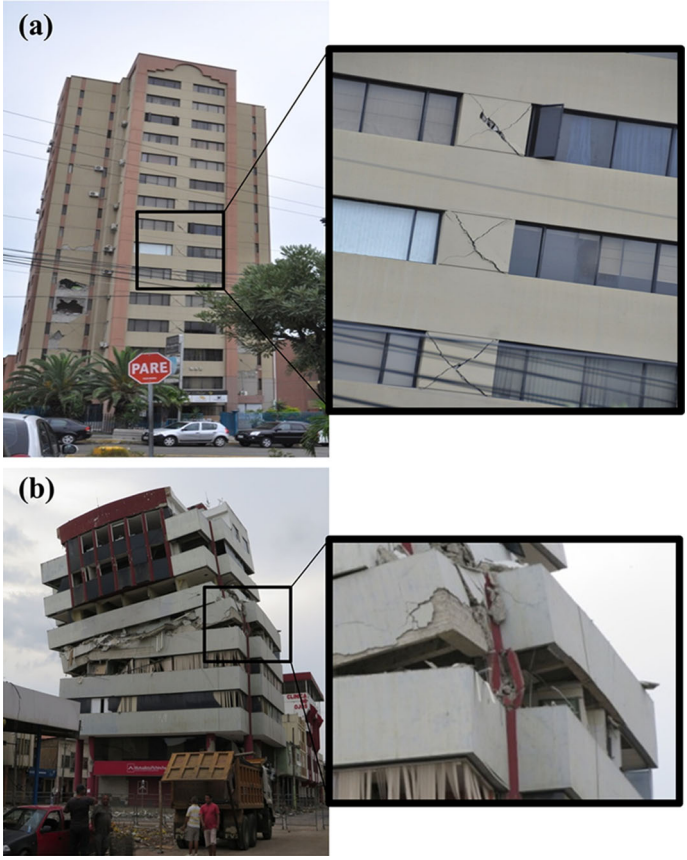

Fig. 11 15-storey RC building in Manta (**a**) and partial collapse of 9-storey RC building in Portoviejo (**b**)

stirrups and lack of transverse confinement, resulting in combined axial-shear failure and buckling of longitudinal reinforcement.

5 Case study

In order to gain better understanding of the observed structural performance and provide quantitative outcome on some structural response parameters, such as maximum displacements, inter-storey drifts (IDR), etc., a number of nonlinear static analyses were performed on a selected case study building, using the recorded ground motions in Pedernales and Manta. It should be noted that reproducing the response of real buildings under earthquake excitation is a challenging task, due to uncertainties in the ground motion and soil conditions at the site, structural material behavior and 3D interaction with structural and non-structural components. Notwithstanding, overall good correlation is found in the present case with the observed damage patterns, such as concrete crushing in the columns, damage to infills and soft-storey mechanisms, among others, highlighting the potential

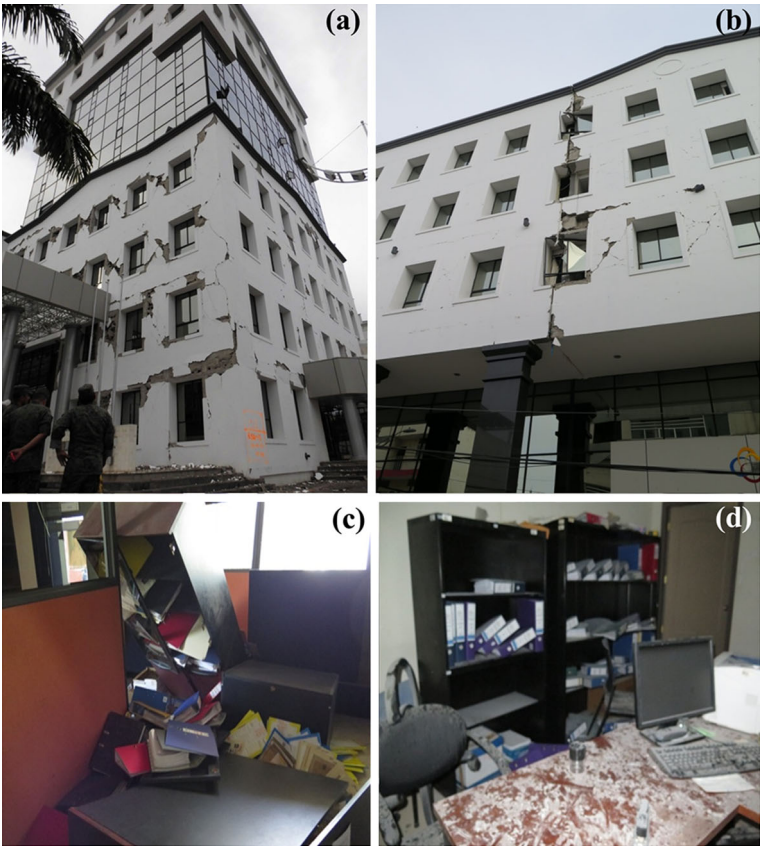

Fig. 12 **a** Exterior damage to the Supreme Court building, **b** pounding at the construction joint, **c** non-structural damage at upper stories and **d** at lower stories

vulnerability of flexible non-ductile RC infilled frames, especially when affected by corrosion.

5.1 Description

The selected case study structure is representative of a typical non-engineered RC building found during the field investigation (Figs. 6, 7, 8). It consists of a three-storey, two- by three-bay RC frame with masonry infills and flat slabs (Fig. 15). The distribution of masonry infills was irregular in plan and elevation, giving rise to torsional stiffness and strength eccentricity, as well as a soft-storey configuration. Three different types of infill openings were considered, corresponding to windows (W), doors (D) and full (F) panels (Fig. 16). Selected results from eigenvalue, pushover and nonlinear time history analysis will be presented herein.

The dimensions of the frame were based on field observations, resulting in 20×20 cm^2 rectangular cross-sections for the columns, 20 cm thick slabs, a maximum clear span of 3.8 m and a clear height of 2.80 m between storeys. All columns were equally reinforced with eight 16 mm bars uniformly distributed around the perimeter and 8 mm stirrups

Fig. 13 **a** Damage to the retrofitted Miguel Hilario Alcivar hospital in Bahía de Caráquez, **b** interior damage to partitions and content, and **c** structural damage in the wall boundary

Fig. 14 **a** Damage to the building tower of the Solca hospital in Portoviejo, **b** failure of a non-structural column, and **c** shear failure of an interior column

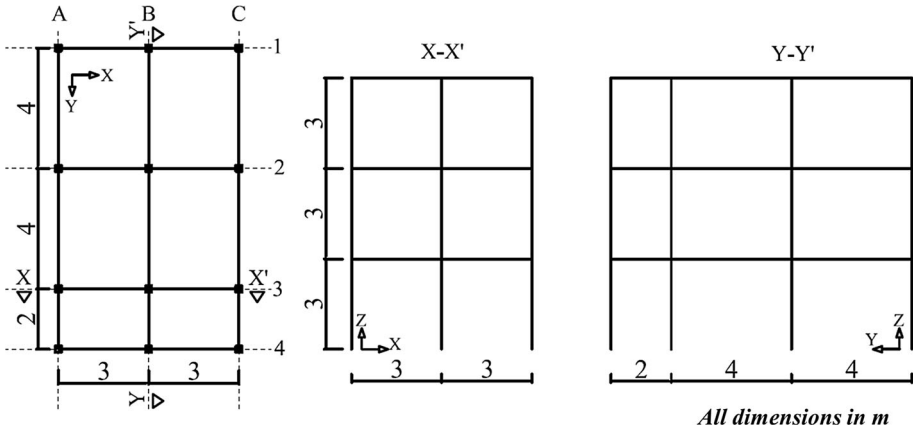

Fig. 15 Plan and elevation of the case study building

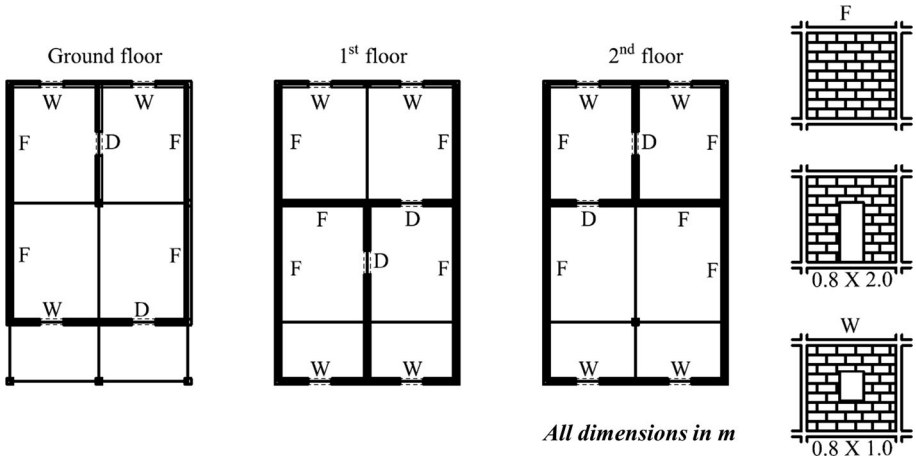

Fig. 16 Distribution of masonry infills in the case study building

spaced at 200 mm. For the slabs, 16 mm bars were assumed in the slab-column region and 8 mm bars in the region outside (Fig. 17). The portion of the slab modeled in the analysis corresponded to its effective width, as explained in the next section, following the

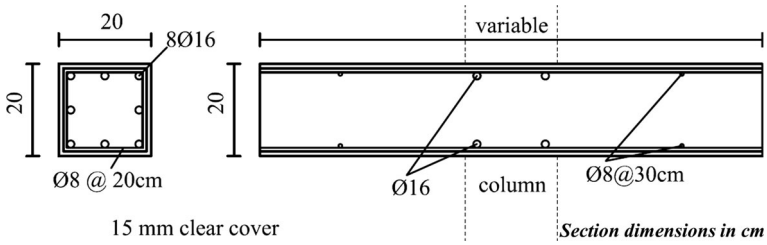

Fig. 17 Cross-section and reinforcement layout of the column and equivalent beams

equivalent beam analogy. For both columns and slabs, a concrete clear cover of 15 mm was adopted. Expected values for the concrete strength, f_{cm}, and yield strength of steel, $f_{y,av}$, were used in the analysis. These were obtained from the characteristic ones as (Comité Europeen de Normalisation 2004):

$$f_{cm} = f_{ck} + 8 = 20 + 8 = 28 \text{ MPa} \quad (1)$$

$$f_{y,av} = 1.1 \times f_{yk} = 1.1 \times 420 = 462 \text{ MPa} \quad (2)$$

Based on field observations, an attempt is made to account for the influence of chloride corrosion in the model response. This is done by reducing the area of longitudinal reinforcement in the members located in the perimeter frames, thus neglecting possible corrosion to internal members due to the use of beach sand aggregates. According to Rasheeduzzafar et al. (1985), a relationship between chloride content, concrete cover and weight loss of reinforcement was found based on a survey of 62 reinforced concrete buildings, between 10 and 12 years old, located in the hot, humid and salty environment along the Arabian Gulf sea cost in Saudi Arabia. These conditions are consistent with the present case. Hence, according to this study and assuming a total chloride content of 2 kg/m^3, the weight loss results to be 40% for a 15 mm concrete clear cover (Fig. 18a).

5.2 Modeling

A three-dimensional finite element model of the frame was created in the computer program IDEEA3D (Kagermanov 2012), using fiber-based beam-column elements. The program uses co-rotational displacement-based finite elements combined with a fiber-section approach for the section discretization, thus fully taking into account geometric and material nonlinearities. Uniaxial hysteretic material models for concrete (Mander et al. 1988) and steel (Menegotto and Pinto 1973) including confinement and Bauschinger effects, among others, were used to model the members of the case study frame.

The frame was assumed fully fixed at the bottom, neglecting soil-structure interaction effects. Four elements per member were used to discretize the columns and beams, being the elements located in the plastic hinge region of shorter length and equal to the plastic hinge length of the member, in order to preserve objectivity. The cross-section was discretized into 100 fibers. Longitudinal reinforcement was defined pointwise according to the layout of the section (Fig. 17). Concrete and steel material properties assigned to each fiber are summarized in Table 2. Unconfined concrete properties were assigned to all of the

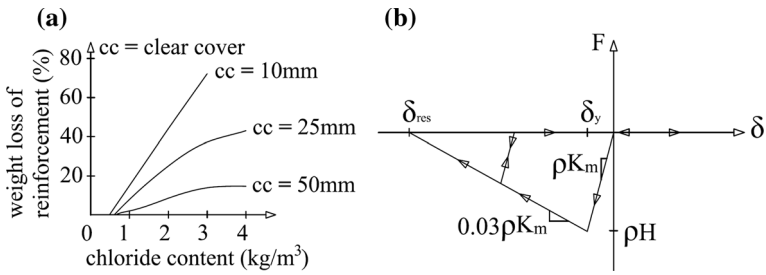

Fig. 18 Percentage of weight loss of reinforcement due to corrosion (Comité Europeen de Normalisation 2004) (**a**) and hysteretic model for the masonry struts (**b**)

Table 2 Concrete and steel material properties

Concrete (unconfined)		Steel	
Compressive strength	$f_c = 28$ MPa	Yield strength	$f_y = 462$ MPa
Peak strain	$\varepsilon_o = 0.002$	Strain hardening ratio	$\mu = 0.005$
Initial Tangent Stiffness	$E_{tg} = 30{,}000$ MPa	Young's Modulus	$E_s = 200.000$ MPa

concrete fibers, since the amount of transverse reinforcement was very low (transverse reinforcement ratio $\approx 0.15\%$).

Slabs were modeled as equivalent beams, whereby an effective width was determined for interior and exterior connections as a function of the span, column dimensions, bending and torsional stiffness (Luo et al. 1994). The effective width varied between 1.2 and 1.5 m for interior connections, and between 0.55 and 0.95 m for the exterior ones. Stiffness reduction due to cracking under gravity loads was assumed as 0.8. The rigid diaphragm action was incorporated with in-plane rigid struts connecting beam-column joints.

Masonry infills were represented by a set of equivalent, compression-only diagonal struts connected between opposite corners of the frame. The hysteretic response of the struts was determined based on Decanini et al. (2004a, b), Fig. 18b, where H and δ_y are the maximum horizontal strength and corresponding displacement, δ_{res} the residual displacement and K_m the initial stiffness of the infill panel. Decanini et al. (2004a, b) propose semi-empirical expressions to evaluate the lateral strength of the panel associated to four types of failure: (1) diagonal tension, (2) shear sliding, (3) corner crushing and (4) compression failure of the strut. Also, the effect of the openings is accounted for through a strength and stiffness reduction factor, ρ, which depends on the relative dimensions of the opening with respect to the panel.

The common type of masonry infills corresponded to $270 \times 70 \times 115$ mm^3 clay brick units with no openings and 10 mm thick cement mortar filling vertical and horizontal joints. The compressive strength of the brick and the mortar were assumed as 5 and 10 MPa, respectively, which are believed to be representative of the relatively low quality of the masonry found on site. The compressive strength of the masonry panel and its stiffness were estimated as 3.9 and 3,900 MPa, respectively, and the sliding shear strength as 0.15 MPa upon neglecting friction due to vertical stresses (Paulay and Priestley 1992). Based on these properties, the critical failure mode for all the panels resulted to be diagonal tension, which is consistent with the field observations.

Masses corresponding to the self-weight of the structural elements and a dead load of 2.5 kN/m^2 were included in the dynamic analysis. These were distributed uniformly in plan and elevation, resulting in a total weight of the building of $W = 1460$ kN. Masses due to the self-weight of columns and beams were modeled as distributed masses (consistent mass matrix), whereas the rest of masses were lumped at the beam column joints (lumped mass matrix). Gravity loads were defined directly from masses at the beam-column nodes, resulting in axial-load ratios of about 4%.

5.3 Analysis results: eigenvalue and pushover

Natural periods, mode shapes and participation masses obtained from eigenvalue analysis are summarized in Table 3, for the bare and infilled frames. These were obtained with

Table 3 Results from eigenvalue analysis

Mode	Bare		Infill and corroded	
	Period (s)	Mass (%)	Period (s)	Mass (%)
1st bending—y	0.68	89	0.22	75
1st bending—x	0.68	87	0.17	92
1st global torsion	0.63	1	0.17	19
2nd bending—y	0.23	9	0.07	4
2nd bending—x	0.23	9	0.06	6
2nd global torsion	0.22	0.1	0.06	1

initial (uncracked) stiffnesses and without consideration of the axial load and corrosion, since the objective was to quantify the effect of the infills. It can be observed the infills shorten the period by a factor of 3–4, depending on the direction of the mode shape. Also, stiffness irregularity introduced by the infills can be appreciated from the difference in periods (and participation mass) between y and x directions for a given bending mode (Fig. 15), e.g. periods of 0.22 and 0.17 s for the 1st bending mode of the infilled frame.

Results from conventional pushover analysis using a triangular lateral load distribution are presented in Figs. 19 and 20. Two pushover curves are presented in each direction for: (1) the infilled frame and (2) the corroded frame with infills and 40% reinforcement cross-section reduction in the perimeter members. Four different limit states were identified along the curves from local response parameters. These correspond to: (1) 0.5% IDR for non-structural damage, (2) local yielding of longitudinal reinforcement, when the tensile strain in any rebar exceeded 2.3‰, labeled as "1st yield", (2) on set of concrete crushing, when the compressive strain any concrete fibers exceeded 2‰, labeled as "Crushing", and (3) when an IDR of 2% was reached in any of the columns, labeled as "2% IDR". Also, the collapse mechanism at maximum base shear for the corroded frames is depicted in Figs. 19 and 20.

All of the pushover curves showed similar type of behavior characterized by cracking, yielding of beams and columns at different locations, compression crushing in the hinges where yielding previously occurred, lateral displacements reaching 2% IDR and finally

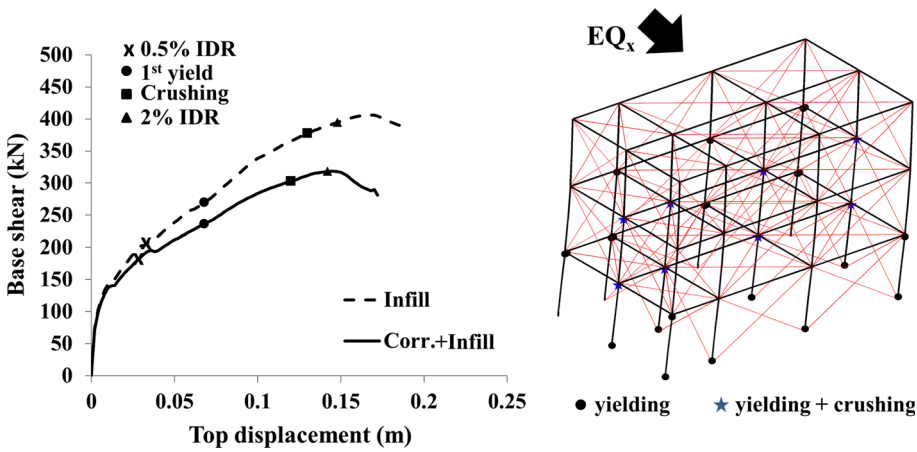

Fig. 19 Pushover curves and collapse mechanism in the x-direction for the infilled and corroded frames

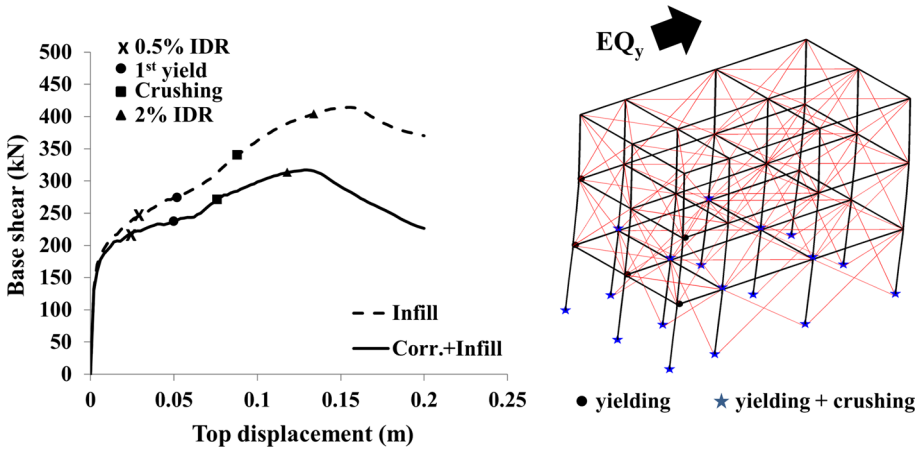

Fig. 20 Pushover curves and collapse mechanism in the y-direction for the infilled and corroded frames

brittle global collapse due to combined p-delta and concrete softening effects. Plastic hinges formed at the base of the ground-floor-columns, as well as in beams and columns at intermediate levels. The roof level was always free from plastic hinges.

For the pushover in the x-direction (Fig. 19), the maximum base shear reached 405kN (0.28 W) and 318kN (0.22 W) for the infilled and the corroded frames, respectively. According to the NEC-2014, the inelastic base shear coefficient in Manta and Pedernales is about 0.25, which is close to the obtained values. For the corroded frame it was noted that more hinges appeared in the columns. The 2% IDR occurred simultaneously at the ground and 1st storey for the infilled frame, whereas it only occurred at the ground storey for the corroded frame, triggering a soft-storey mechanism. In all cases, crushing at the top of the intermediate columns (B1, B2, B3 and B4) at the ground and 1st storey took place.

For the pushover in the y-direction (Fig. 20), the initial stiffness was higher and the displacement at 1st first yield somewhat lower, due to the larger number of bays and infills activated in this direction. The maximum base shear was similar to that in the x-direction, and the corresponding displacement slightly lower. The number of plastic hinges was the same for the two frames, being most of them located at the bottom of the ground-floor-columns. For the corroded frame, also crushing in the previously yielded hinges was observed. The 2% IDR was reached at the ground storey only, for both frames, accentuating the soft-storey mechanism in the y-direction.

5.4 Nonlinear performance assessment

In this section, the structural performance of the corroded frame was further assessed using the N2-method (Fajfar 2000). The capacity curves were bilinearized taking the secant through the point of first yield, placing a horizontal cap on the maximum base shear and taking the ultimate displacement as the maximum displacement. This resulted in a secant period of $T^* = 0.98$ s (x-direction) and $T^* = 0.87$ s (y-direction), and a ductility capacity of $\mu_c = 1.6$ (x-direction) and $\mu_c = 1.9$ (y-direction). Higher μ_c was obtained in the y-direction because of the lower yield displacement, as previously discussed. The capacity curves were transformed to the equivalent single degree of freedom system in the acceleration (S_a)—displacement (S_d) spectrum domain, and compared against the inelastic

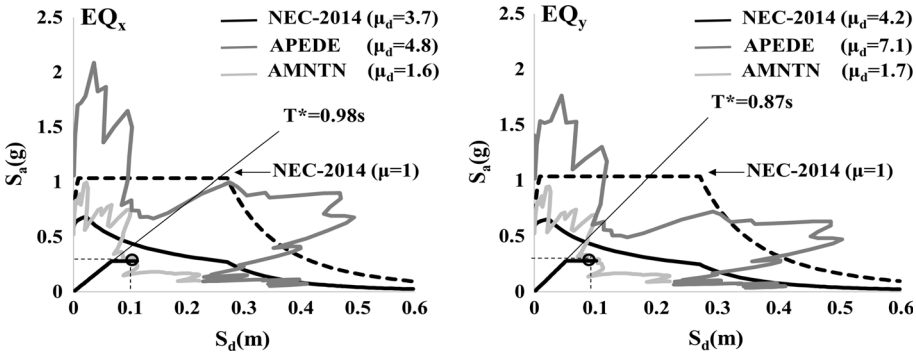

Fig. 21 Performance assessment of the infill frame in x-direction (*left*) and y-direction (*right*)

Table 4 Parameters for nonlinear performance assessment

	x-direction			y-direction		
	NEC-2014	APEDE	AMNTN	NEC-2014	APEDE	AMNTN
R_μ	3.7	4.6	1.6	3.7	6.1	1.7
μ_d	3.8	4.8	1.6	4.2	7.1	1.7
T_c(s)	1.03	1.03	0.62	1.03	1.03	0.62

spectrums from the design code (NEC-2014 Soil-D) and those recorded in Manta (AMNTN) and Pedernales (APEDE) (Fig. 21). Table 4 reports the calculated force reduction factor (R_μ), ductility demand (μ_d) and adopted corner periods (T_c). Note that for the AMNTN record, the secant period (T*) is greater than the corner period (T_c), hence the equal displacement rule applies. i.e. $R_\mu = \mu_d$.

Results in Fig. 21 clearly highlight the insufficient capacity of the structure to sustain the imposed inelastic demands. For the NEC-2014 and the Pedernales spectrums, no intersection with the capacity curve occurs. Only for the Manta record the structure can supply enough ductility to resist the imposed displacements. The corresponding SDOF displacements at the performance point were about 11 and 9 cm in the x and y directions, respectively. For the MDOF, this results in 14 and 11 cm of lateral top displacement, respectively. At this point, most of the limit states have been exceeded and the structure is very close to losing its vertical load carrying capacity (Figs. 19, 20).

6 Conclusions

The Muisne Earthquake of April 2016 was an expected event consistent with the seismological setting of the subduction region in western Ecuador. At the station closest to the epicenter, the recorded peak ground acceleration exceeded that of the seismic hazard map at 475 years return period. In the populated cities of Manta and Portoviejo, spectral accelerations were relatively close to the design level, although local site amplification was observed in Portoviejo at about 0.5 s. The earthquake produced widespread damage and total collapse of several RC structures. The majority of the collapsed structures were not

compliant with seismic design codes. Unfortunately, most of them were residential and commercial buildings with many people at the time of the earthquake. Structures that were compliant with current or recent versions of the Ecuadorian Building Code, and where ground accelerations were not excessively high, satisfied collapse prevention, with a few exceptions where common mistakes of irregularity and lack of ductility resulted in partial collapse. The authors summarize the following deficiencies observed during their field investigations:

- Stiff slabs with slender columns, resulting in large frame flexibility and excessive drifts demands.
- Insufficient transverse confinement in columns, hooks bent at 90° instead of 135° and excessive spacing between stirrups in the plastic hinge regions, resulting in axial-shear failures and buckling of longitudinal reinforcement.
- Deficient detailing of slab-to-column connections and formation of plastic hinges in columns. Insufficient anchorage length.
- Heavy partitions, cladding panels and plaster covers increased gravity loads and p-delta effects.
- Limited use of shear walls. This could have prevented excessive drifts and associated cost of demolition and repair due to permanent drifts and non-structural damage.
- Structural alterations such as soft-storeys at the ground level and addition of extra storeys at separate construction stages.
- Insufficient concrete cover, use of beach sand as a concrete aggregate and corrosion of reinforcement.
- Use of unconfined, unreinforced masonry infills. Neither appropriate connection nor separation from the surrounding RC frame, resulting in many in-plane and out-of-plane failures.

Numerical analysis included in the paper pointed out some of the deficiencies listed above. In particular, in-plane damage to the infills occurring much earlier than yielding of the frame, the formation of plastic hinges in the columns and soft-storey mechanisms, and the negative post-peak stiffness due to the large frame flexibility and p-delta effects. The impact of corrosion was quantified as almost 30% reduction in maximum base shear.

It is noted that the objective of the numerical study was not to evaluate or suggest improvements to the current Ecuadorian Building Code. This task would require further detailed studies. In the authors' opinion the current Ecuadorian Building Code (NEC-2014) is in accordance with the international state of practical knowledge in seismic design, and it is rather its application and enforcement from local authorities which requires further improvement.

Acknowledgements The authors are very grateful to the Corps of Engineers of the Ecuadorian Army. In particular, Cor. Ramos, Cor. Riofrío, Gen. Mosquera and Ing. Romo. Also, Dr. Roberto Aguiar from the Polytechinc Engineering School of the Ecuadorian Army (ESPE), the Institute of Geophysics of Ecuador (IGEPN) and Prof. André Filiatrault (University of Buffalo, NY). The authors appreciate the valuable suggestions from Robin Gee (Global Earthquake Model, Pavia) and Prof. Julian Bommer (Imperial College, London) during the preparation of the manuscript.

References

Abrahamson N, Gregor N, Addo K (2016) BC hydro ground motion prediction equations for subduction earthquakes. Earthq Spectra 32(1):23–44

ASCE (American Society of Civil Engineers) (2010) Minimum design loads for buildings and 355 other structures. In: ASCE/SEI 7-10, Reston, VA

Comité Europeen de Normalisation (2004) Eurocode 8. Design for structures for earthquake resistance—part 1: general rules, seismic actions and rules for buildings. In: EN 1998-1, CEN, Brussels, Belgium

Decanini L, Liberatore L, Mollaioli F (2004a) Strength and stiffness reduction factors for infilled frames with openings. Earthq Eng Eng Vib 13(3):437–454

Decanini L, Mollaioli F, Mura A, Saragoni R (2004b) Seismic performance of masonry infilled RC frames. In: 13th world conference on earthquake engineering, Vancouver, Canada

Earthquake Engineering Research Institute (2016a) Learning from earthquakes: the Bahía de Caráquez, Ecuador, Eathquake of August 4, 1998. EERI special earthquake report. http://www.eeri.org/. 20 May 2016

Earthquake Engineering Research Institute (2016b) 1987 Ecuador earthquakes of March 5, 1987. EERI Special Earthquake Report. http://www.eeri.org/. 20 May 2016

Fajfar P (2000) A nonlinear analysis method for performance based seismic design. Earthq Spectra 16(3):573–592

Harp EL, Wilson RC (1995) Shaking intensity thresholds for rock falls and slides: evidence from Whittier Narrows and Superstition Hills earthquake strong-motion records. Bull Seismol Soc Am 85:1739–1757

Instituto Geofísico Escuela Politécnica Nacional de Ecuador (IGEPN) (2016) http://www.igepn.edu.ec/. 20 May 2016

Instituto Nacional de Estadística y Censos INEC (2016a) Anuario estadístico 2013. Análisis. http://www.ecuadorencifras.gob.ec. 10 May 2016

Instituto Nacional de Estadística y Censos INEC (2016b) Resultados del censo 2010 de población y vivienda en el Ecuador. Fascículo provincial Manabí. http://www.ecuadorencifras.gob.ec. 10 May 2016

Instituto Nacional de Estadística y Censos INEC (2016c) Resultados del censo 2010 de población y vivienda en el Ecuador. Fascículo provincial Esmeraldas. http://www.ecuadorencifras.gob.ec. 10 May 2016

Instituto Nacional de Estadística y Censos INEC (2016d) Resultados del censo 2010 de población y vivienda en el Ecuador. Fascículo provincial Santo Domingo. http://www.ecuadorencifras.gob.ec. 10 May 2016

Kagermanov A (2012) IDEEA3D: inelastic dynamic analysis for earthquake engineering applications. https://sites.google.com/site/ideeanalysis/. 10 Jan 2012

Luo YH, Durrani AJ, Conte JP (1994) Equivalent frame analysis of flat plate buildings for seismic loading. J Struct Eng 120(7):2137–2155

Mander JB, Priestley MJN, Park R (1988) Theoretical stress–strain model for confined concrete. J Struct Eng 114(8):1804–1826

McVerry GH, Zhao JX, Abrahamson NA, Somerville PG (2006) New Zealand acceleration response spectrum attenuation relations for crustal and subduction zone earthquakes. Bull N Z Soc Earthq Eng 39(1):1–58

Menegotto M, Pinto PE (1973) Method of analysis of cyclically loaded reinforced concrete plane frames including changes in geometry and non-elastic behavior of elements under combined normal force and bending. In: IABSE symposium, resistance and ultimate deformability of structures acted on by well-defined repeated loads, IABSE, Zurich, Switzerland

Neinhuys S, Naranjo C, Estrada R (1976) Guía Popular de Construcción Sismoresistente. Instituto Ecuatoriano de Normalización, Diciembre, Quito, Ecuador

Norma Ecuatoriana de la Construcción (2014) Peligro Sísmico. Diseño Sismoresistente. Ministerio de Desarrollo Urbano y Vivienda, Quito, Ecuador

Paulay T, Priestley MJN (1992) Seismic design of reinforced concrete and masonry buildings. Wiley, Hoboken

Rasheeduzzafar D, Fahd H, Ahtani G, Ahmad S (1985) Corrosion of reinforcement in concrete structures in the Middle East. Concr Int Des Constr 7(9):48–55

Secretaría de Gestión de riesgos (2016) Ecuador. Informe de Situación N° 57 (03-05-2016) 18H:00 Terremoto 7.8 Pedernales. http://www.gestionderiesgos.gob.ec/. 10 May 2016

Strasser FO, Arango MC, Bommer JJ (2010) Scaling of the source dimensions of interface and intraslab subductionzone earthquakes with moment magnitude. Seismol Res Lett 81(6):941–950

US Geological Survey (2016) M7.8—29 km SSE of Muisne, Ecuador. http://earthquake.usgs.gov/earthquakes/eventpage/us20005j32#general. 20 May 2016

United Nations Institute for Training and Research UNITAR (2016) Ecuador earthquake preliminary satellite based damage assessment report. http://www.unitar.org/. 10 May 2016

Wikipedia the Free Encyclopedia (2016) https://es.wikipedia.org/wiki/. 25 May 2016